Super-resolution imaging by one-dimensional, microwave left-handed metamaterials with an effective negative index

Ekmel Ozbay[1,2]**, Zhaofeng Li**[1] **and Koray Aydin**[1]

[1] Nanotechnology Research Center and Department of Physics, Bilkent University, Bilkent, 06800 Ankara, Turkey
[2] Department of Electrical and Electronics Engineering, Bilkent University, Bilkent, 06800 Ankara, Turkey

E-mail: ozbay@bilkent.edu.tr and aydin@fen.bilkent.edu.tr

Abstract
Superlenses based on metamaterials are promising candidates for achieving subwavelength resolution. We report here our experimental studies on super-resolution imaging from one-dimensional (1D) negative index metamaterial superlenses at microwave frequencies. The metamaterial structure under investigation is shown to have a left-handed transmission band at frequencies where both effective permittivity and permeability are negative. The retrieved effective parameters are in good agreement with the measurements. We achieved a resolution of 0.2λ by imaging a single point source from a 1D superlens. Moreover, the effect of the superlens' thickness on the resolution is studied. A thicker superlens suffers from more losses, which in turn reduces the resolution. Two point sources that were separated by distances that were smaller than a half-wavelength were successfully resolved with the negative index superlens.

(Some figures in this article are in colour only in the electronic version)

1. Introduction

The electromagnetic responses of materials are characterized by dielectric permittivity (ε) and magnetic permeability (μ). Permittivity is responsible for the electric response, whereas the permeability determines the magnetic response of materials. In recent years, there has been a growing amount of interest in tailoring these parameters by means of artificially engineered structures, or so-called metamaterials [1–18]. Metamaterials enable us to obtain the desired values of ε and μ that are not readily available in ordinary materials. Since the refractive index of a medium is determined by its permittivity and the permeability by the formula $n^2 = \varepsilon\mu$, negative values of a refractive index are accessible by virtue of metamaterial structures that simultaneously possess negative values of permittivity [2] and permeability [3]. The choice of the appropriate sign of refractive index is negative when ε and μ are simultaneously negative, as was clearly described by Ziolkowski and Heyman [5]. Inside a left-handed medium, group and phase velocities are anti-parallel, in which case the wavevector ($\mathbf{k}$), electric field ($\mathbf{E}$), and magnetic field ($\mathbf{H}$) all obey the left-hand rule [1].

Negative refraction is also achievable with two-dimensional (2D) photonic crystals (PC) [19–25]. However, the periods of PCs are on the order of the wavelength, meaning that an effective index cannot be assigned. PCs have photonic bands that exhibit different dispersions for the propagation of electromagnetic waves and band gaps where wave propagation is prohibited in a certain frequency range [27–36]. In photonic crystals, the permittivity is positive and modulated wherein the periodicity and permeability is unity. Negative refraction in photonic crystals is obtained via different mechanisms, such as band structures that exhibit negative dispersion for electromagnetic waves or anisotropy in wavevector space [24].
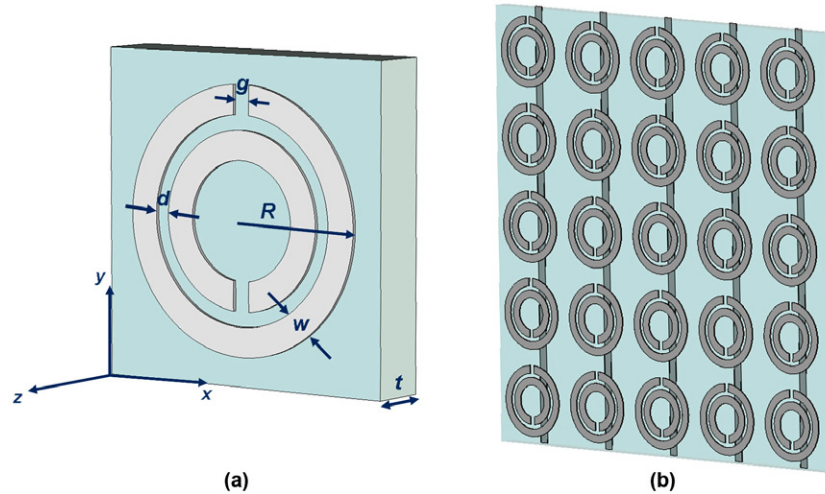
Figure 1. Schematic drawing of a single layer of LHM. Split ring resonators are printed on the front side, and the wires on the back side. Directions are shown in the left-bottom corner.

However, in metamaterials, negative refraction is achieved by engineering structures to exhibit negative permittivity and negative permeability over a certain frequency regime. Superlensing in photonic crystals have been demonstrated in the near-field zone experimentally [22, 23]. However, Wang *et al* [25] showed the possibility to achieve unrestricted superlensing, satisfying in turn the conditions that are provided in [24].

Metamaterials offer counterintuitive phenomena that are not achievable with common materials. One of the most exciting applications of metamaterials is a superlens. In his seminal paper, Pendry discussed the possibility of obtaining subwavelength imaging by virtue of metamaterials [37]. Negative index media restore the evanescent components of the electromagnetic wave. The details of the image are carried by the high-k components of the evanescent field and the contribution of these higher order modes to the imaging process then results in a better resolution. Metamaterial based superlenses are demonstrated to resolve subwavelength features at microwave [38–40] and optical frequencies [41–44]. Hyperlenses are also promising, since they magnify smaller objects by using cylindrically shaped metamaterial structures with a hyperbolic dispersion [45–47]. Metamaterials also pave the way towards cloaking devices. Theoretical [48] and experimental [49] studies reveal the possibility of cloaking coatings that allow the electromagnetic wave to pass around the cloaked object. Metamaterial research was started at microwave frequencies, but there has been a significant amount of work carried out to scale down metamaterial structures for operation at terahertz and optical frequencies [50–53].

In the present work, we focused on the superlens application of negative index metamaterials at microwave frequencies. The metamaterials under investigation are one-dimensional periodic stacks of alternating split ring resonator and wire arrays. The left-handed transmission region is verified by measured and simulated transmission coefficients. The retrieved effective parameters showed that our structure has negative permittivity and permeability at the left-handed transmission band and the effective index is found to be negative. We have been able to resolve a point source with a resolution of 0.2λ by using a negative index based superlens.

2. Left-handed transmission band

The most common left-handed material design is the periodic arrangement of split ring resonators with wire arrays. It is well known that periodic SRR arrays provide negative values of permeability close to the magnetic resonance frequency of SRR. Negative permittivity is achieved with the periodic arrangement of thin wire arrays. Here, we review the transmission properties of SRR and the corresponding LHM structure. A split ring resonator is schematically shown in figure 1(a). SRR parameters are $d = g = 0.2$ mm, $w = 0.9$ m, and $R = 3.6$ mm. The substrate is a lossy FR4 circuit board with a thickness of $t = 1.6$ mm. The metal part is copper. The split ring resonator and wire patterns are fabricated on the front and back sides of FR4 printed circuit boards as is schematically shown in figure 1(b). The width of the wire is 0.9 mm [8]. The left-handed material is composed of $N_x = 5$, $N_y = 15$, and $N_z = 32$ unit cells, with lattice spacings $a_x = a_y = 8.8$ mm and $a_z = 6.5$ mm.

Transmission measurements were carried out by using an HP-8510C network analyzer and two horn antennae. The distance between the antennae was 50 cm. The transmission results are calibrated with respect to the transmission in free space. In the measurements, the wavevector is along the x axis, the E-field is along the y axis, and the H-field is along the z axis. Figure 2 shows the measured transmission spectra of SRR (black line) and LHM (blue line). A band gap between 3.55 and 4.05 GHz is observed in the transmission spectrum of SRR. In previous work, we have shown that the band gap at these frequencies is caused by the strong magnetic response of SRR to the incident electromagnetic field [8]. The plasma frequency of the wire array, which is used to construct the left-handed material, is at 8.0 GHz. Since the effective permittivity possesses negative values below the plasma frequency one can easily construct a left-handed metamaterial ensuring that
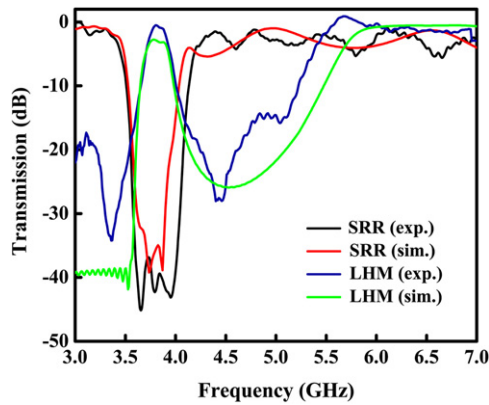
Figure 2. Measured and simulated transmission spectra of periodic SRR and LHM structures.

Figure 3. Measured transmission (blue line) and reflection (red line) spectra of periodic LHM.

the negative permittivity region coincides with the negative permeability region [8]. For our structure, both electric permittivity and magnetic permeability are negative between 3.55 and 4.05 GHz. As expected, a transmission band with left-handed electromagnetic propagation appears at the frequency range of 3.55–4.05 GHz. The transmission peak is measured to be −0.8 dB at 3.86 GHz, which is the highest transmission peak measured for an LHM structure at microwave frequencies. The high transmission could be attributed to the matched impedance, which will discuss in detail later. We also performed numerical simulations by using the commercially available software, CST MICROWAVE STUDIO. In the simulations, a 5 layer LHM structure was subjected to the plane wave and the E-field along the y direction was probed at a distance from the metamaterial. Periodic boundary conditions were applied along the y and z axes. Along the propagation direction (x axis), we applied open boundary conditions. The simulated transmission spectra for SRR and LHM are shown in figure 2 as red and green lines, respectively. The band gap of SRR in the simulated transmission spectrum appears at the same frequency region when compared with the measured transmission spectrum. In the simulations, the left-handed transmission band was observed between 3.60 and 4.10 GHz with a peak value of −2.7 dB.

Figure 3 plots the measured reflection spectrum of 1D LHM together with its transmission spectrum. As seen in the figure, a sharp dip is observed in the reflection spectrum at 3.75 GHz. The reflection is −40 dB at this frequency. Incident electromagnetic waves do not face a significant amount of reflection from the LHM surface for normal angles of incidence. This low reflection regime is due to the matched impedance between the LHM structure and air. Impedance matching will be discussed in the following section.

3. Retrieved effective parameters

Dielectric permittivity, $\varepsilon = \varepsilon' + i\varepsilon''$ and magnetic permeability, $\mu = \mu' + i\mu''$ are used to describe the response of materials to the incident electromagnetic field; where ε' and μ' are the real parts, and ε'' and μ'' are the imaginary parts of the

corresponding effective parameters. The retrieval procedure is widely used to extract the effective parameters of metamaterial structures [54–56]. The effective parameters of the NIM are retrieved by using the calculated amplitudes and phases of transmission and reflection. We employed the retrieval procedure in order to obtain the effective parameters Z_{eff}, n_{eff}, $\varepsilon_{\mathrm{eff}}$, and μ_{eff} by following the approach as outlined in [55]. The advantage of this procedure is that the correct branch of the effective refractive index and effective impedance was selected. The ambiguity in the determination of the correct branch is resolved by using an analytic continuation procedure. The S parameters are simulated by using HFSS, which is a full-wave electromagnetic software program whose accuracy has been verified earlier [54]. For the HFSS simulations, a single unit cell is simulated along the x direction, with periodic boundaries applied along the y and z directions. Therefore, the simulation setup coincides with a slab of LHM, which consists of a single layer. The effective permittivity and permeability values were then derived from the transmission and reflection coefficients of the single layer of LHM. The transmission (red line) and reflection (blue line) spectra of a single unit cell of LHM are plotted in figure 4(a). The transmission peak and reflection dip appear at 3.85 GHz. These data together with the calculated transmission and reflection phase data are used to extract the effective index and effective impedance of the LHM media. The real (blue line) and imaginary (red line) parts of the effective refractive index are shown in figure 4(b). The refractive index possesses negative values between 3.50 and 4.20 GHz. This frequency region coincides with the left-handed transmission band that was observed from the measurements and CST simulations. Figure 4(c) shows the real (blue line) and imaginary (red line) parts of the effective impedance of the composite LHM.

Once we find the effective index and impedance of the system, the effective permittivity and permeability can be calculated by using the relations, $\varepsilon = n/Z$ and $\mu = nZ$ [54]. We plotted the real (blue line) and imaginary (red line) parts of the effective permittivity and permeability of the medium in figures 5(a) and (b), respectively. As expected, the dielectric permittivity of the composite medium is negative below the plasma frequency. Near the resonance frequency of SRR
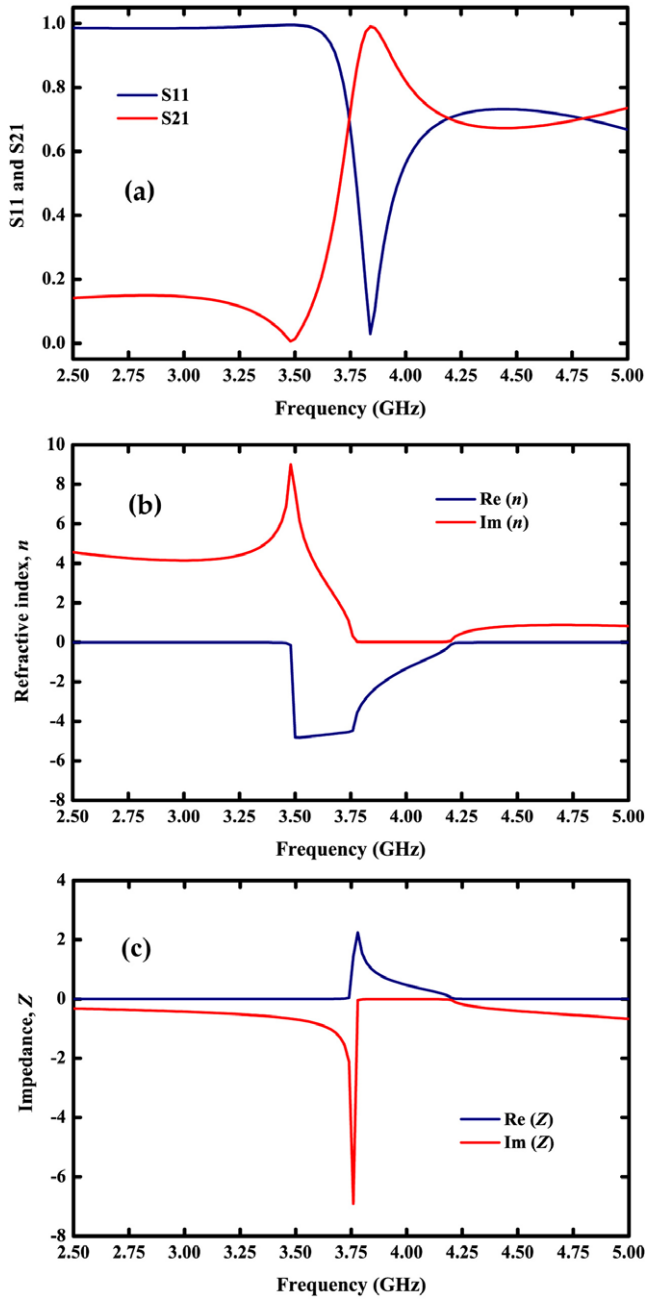
3

Figure 4. Simulated (a) *S*-parameters, (b) real and imaginary parts of refractive index, (c) real and imaginary parts of impedance for one-dimensional left-handed metamaterial.

Figure 5. Simulated real and imaginary parts of effective (a) dielectric permittivity and (b) magnetic permeability.

(3.85 GHz), the form of the permittivity deviates from the Drude model [54]. The effective permeability possesses both positive and negative high values around the magnetic resonance frequency. Permeability is negative between 3.75 and 4.20 GHz.

For a better interpretation of the retrieved effective parameters, we plot the real parts of the effective permittivity, permeability, refractive index, and impedance in figure 6. ε' and μ' possess negative values between 3.75 and 4.20 GHz. The minimum reflection in the simulations occurs at 3.85 GHz, where $\varepsilon' = \mu' = -2.45$ (dashed gray line). The impedance is defined as $Z' = \sqrt{\mu'/\varepsilon'}$ and, therefore, impedance matching
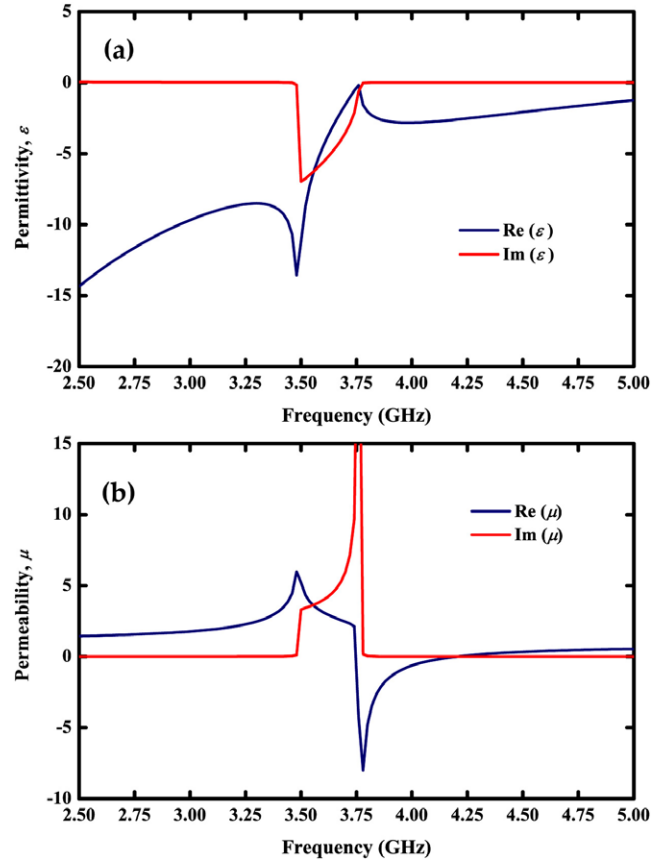
is obtained when $\varepsilon' = \mu'$. This frequency corresponds to the minimum of the reflection spectrum and, therefore, the impedance of LHM is matched to that of free space at 3.85 GHz (dashed line in figure 6), where $Z' = 1$. The refractive index is, $n' = -2.45$ at 3.85 GHz. The imaginary part of the effective index is $n'' = 0.012$, which means that the losses are small at the frequency of the minimum reflection. The ratio of the absolute value of the real part of the index to its imaginary part is a figure of merit for negative index metamaterials. For our metamaterial structure, the figure of merit is calculated as FOM $= |n'|/n'' = 205$. In a previous work we reported an FOM of 12 for a 2D LHM [40]. The minimum reflection frequency is observed at 3.75 GHz in the measurements. However, in the simulations it appeared at 3.85 GHz. This frequency difference between the simulated and measured reflection spectrum may be attributed to fabrication tolerances and a deviation from the ideal structure that may possibly be caused by misalignments during the experiments.

4. Super-resolution imaging by using LHM flat lenses

As discussed in the previous section, at 3.75 GHz, the reflection is very low and, therefore, losses due to reflection can be neglected. Therefore, we targeted the frequency of 3.75 GHz in the imaging experiments. A monopole antenna was used as an emitter in the experiments in order to imitate
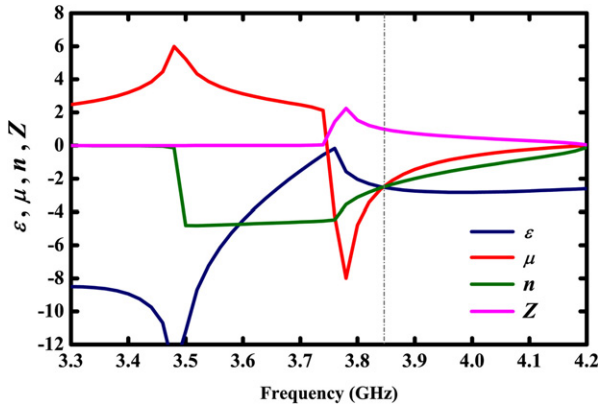
Figure 6. Simulated real parts of effective permittivity, permeability, refractive index, and impedance. The dashed gray line corresponds to the frequency region where $\varepsilon = \mu$, and therefore the impedance is $Z = 1$.
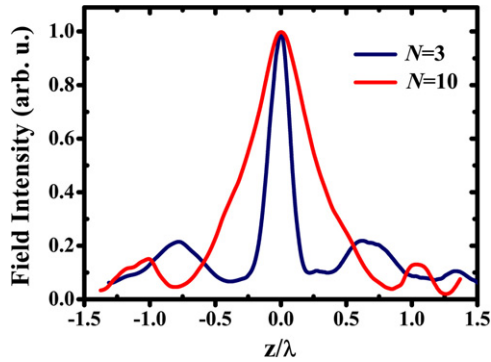

Figure 7. Measured field intensity at the image plane of superlenses with 3 and 10 layers along the propagation direction.
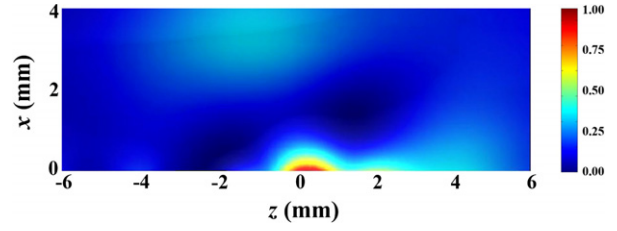

Figure 8. Electric field intensity scan along the lateral and longitudinal axes from the LHM superlens with 3 unit cells along the propagation direction (x). The point $x = 0$ corresponds to an image plane of the superlens that is 0.8 cm away from the boundary of the superlens.
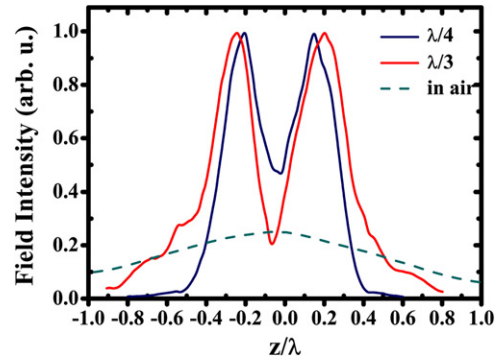

Figure 9. Measured beam profiles at the image plane of superlens with two point sources separated by the distances $\lambda/4$ (blue line) and $\lambda/3$ (red line). The dashed green line corresponds to the beam profile without an LHM superlens, in which the distance between the sources is $\lambda/3$.

the point source. The exposed center conductor acts as the transmitter and receiver, and has a length of 4 cm ($\sim\lambda/2$). The monopole antenna was aligned parallel to the y-axis in the experiments. The source was placed 1 cm away from the first interface. The beam profile was scanned at the image plane that was 0.8 cm away from the boundary of the superlens. The intensity of the electric field at the image plane was scanned by the receiver monopole antenna with $\Delta x = 2$ mm steps. In the experiments, we employed two LHM superlenses with different thicknesses; LHMs with 3 and 10 layers along the propagation direction (x). The beam profile imaged from a 3 layered LHM superlens is shown as a blue line in figure 7. The full width at half maximum (FWHM) was measured as 0.20λ, which is well below the diffraction limit. The FWHM of the image from a 2D LHM was reported as 0.13λ in a previous work [40]. Thus, the imaging performance of higher dimensional superlenses is better. We also measured the beam profile from a 10 layered LHM (red line), in which the FWHM was found to be 0.55λ, which is just above the diffraction limit. Increasing the thickness of the superlens increases the losses, which in turn results in the shown decrease in the resolution.

We performed a two-dimensional scan for the beam profile starting from the second boundary of the 3 layer superlens. The step sizes are 0.2 mm both along x (longitudinal) and z (lateral)

axes. As seen in figure 8, the image is formed at the exit surface of the LHM superlens. Note that $x = 0$ point is the plane that was 0.8 cm away from the superlens–air interface and corresponds to the image plane of the superlens. The faint image above the image plane might be possibly due to the scattering from the environment.

We have shown that our superlens is able to image a point source. We took a further step and used two point sources that were separated by distances that were smaller than a half-wavelength. In the experiments, two independent signal generators were employed and a microwave spectrum analyzer was used for the detection of the power distribution. The frequencies of the sources differed by 1 MHz in order to ensure that the sources were entirely incoherent. The imaging experiments were performed for two different separation distances between the sources. The measured power distribution of the sources, which were separated by $\lambda/4$, is shown as a blue line in figure 9. As seen in the figure, the peaks of two sources are resolved. The distance between the two peaks is measured as 0.35λ, whereas the sources are separated by 0.33λ. The difference can be attributed to the alignment of the LHM superlens with respect to the source and receiver antennae. When the sources are $\lambda/3$ apart (red line), the resolution improves.

We performed similar imaging measurements at a higher frequency, 6.0 GHz, which is a right-handed transmission
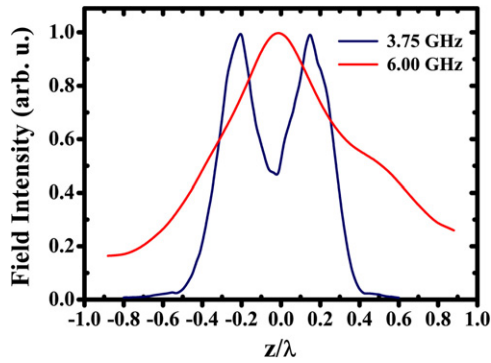
Figure 10. Measured beam profile at the image plane with the sources separated by $\lambda/4$ at the frequencies 3.75 GHz (blue line) and 6.00 GHz (red line).

region (see figure 2). The separation of the sources was $\lambda/4$ and the resulting beam profile is plotted as a red line in figure 10. As is clearly seen in the figure, we were not able to resolve the sources when the refractive index is positive.

5. Conclusions

In the present work, we presented left-handed metamaterial superlenses constructed from a one-dimensional periodic arrangement of split ring resonators and thin wire media. The measurements and simulations predict a band gap at the transmission spectra of SRR arrays. We observed a transmission band that had left-handed propagation characteristics when SRRs are inserted into a negative permittivity media of thin wires. The reflection measurements showed that our LHM structure exhibits low reflection at a certain frequency. This low reflection is due to the impedance matching between LHM and free space, which is supported by the retrieved effective impedance calculations. The impedance becomes unity at this low reflection frequency. The effective index is shown to be negative at a frequency region where the effective permittivity and permeability of the LHM are simultaneously negative. A one-dimensional superlens was used to image a point source that is clearly a subwavelength object. The effect of the thickness on the resolving power was studied, in which the thicker lenses were shown to have a lower resolution compared to thinner lenses. We also performed measurements with two point sources that were separated by a distance that was smaller than half wavelengths. We were able to resolve two objects that were $\lambda/4$ apart.

Acknowledgments

References

[1] Veselago V G 1968 *Sov. Phys.—Usp.* **10** 509
[2] Pendry J B, Holden A J, Robbins D J and Stewart W J 1998 *J. Phys.: Condens. Matter* **10** 4785
[3] Pendry J B, Holden A J, Robbins D J and Stewart W J 1999 *IEEE Trans. Microw. Theory Tech.* **47** 2075
[4] Smith D R, Padilla W J, Vier D C, Nemat-Nasser S C and Schultz S 2000 *Phys. Rev. Lett.* **84** 4184
[5] Ziolkowski R W and Heyman E 2001 *Phys. Rev.* E **64** 056625
[6] Shelby R A, Smith D R and Schultz S 2001 *Science* **292** 77
[7] Wiltshire M C K, Pendry J B, Young I R, Larkman D J, Gilderdale D J and Hajnal J V 2001 *Science* **291** 849
[8] Aydin K, Guven K, Kafesaki M, Zhang L, Soukoulis C M and Ozbay E 2004 *Opt. Lett.* **29** 2623
[9] Katsarakis N, Koschny T, Kafesaki M, Economou E N and Soukoulis C M 2004 *Appl. Phys. Lett.* **84** 2943
[10] Aydin K, Guven K, Soukoulis C M and Ozbay E 2005 *Appl. Phys. Lett.* **86** 124102
[11] Gokkavas M, Guven K, Bulu I, Aydin K, Penciu R S, Kafesaki M, Soukoulis C M and Ozbay E 2006 *Phys. Rev.* B **73** 193103
[12] Penciu R S, Kafesaki M, Gundogdu T F, Economou E N and Soukoulis C M 2006 *Photon. Nanostruct. Fundam. Appl.* **4** 12
[13] Aydin K, Bulu I and Ozbay E 2006 *Microw. Opt. Technol. Lett.* **48** 2548
[14] Katsarakis N, Kafesaki M, Tsiapa I, Economou E N and Soukoulis C M 2007 *Photon. Nanostruct. Fundam. Appl.* **5** 149
[15] Aydin K and Ozbay E 2007 *Appl. Phys.* A **87** 137
[16] Gundogdu T F, Gokkavas M, Guven K, Kafesaki M, Soukoulis C M and Ozbay E 2007 *Photon. Nanostruct. Fundam. Appl.* **5** 149
[17] Aydin K and Ozbay E 2007 *J. Appl. Phys.* **101** 024911
[18] Wood B and Pendry J B 2007 *J. Phys.: Condens. Matter* **19** 076208
[19] Notomi M 2000 *Phys. Rev.* B **62** 10696
[20] Luo C, Johnson S G, Joannopoulos J D and Pendry J B 2002 *Phys. Rev.* B **65** 201104
[21] Cubukcu E, Aydin K, Ozbay E, Foteinopoulou S and Soukoulis C M 2003 *Nature* **423** 604
[22] Cubukcu E, Aydin K, Ozbay E, Foteinopolou S and Soukoulis C M 2003 *Phys. Rev. Lett.* **91** 207401
[23] Guven K, Aydin K, Alici K B, Soukoulis C M and Ozbay E 2004 *Phys. Rev.* B **70** 205125
[24] Foteinopoulou S and Soukoulis C M 2005 *Phys. Rev.* B **72** 165112
[25] Wang X, Ren Z F and Kempa K 2004 *Opt. Express* **12** 2919
[26] Yablonovitch E 1987 *Phys. Rev. Lett.* **58** 2059
[27] John S 1987 *Phys. Rev. Lett.* **58** 2486
[28] Ozbay E, Michel E, Tuttle G, Biswas R, Ho K M, Bostak J and Bloom D M 1994 *Appl. Phys. Lett.* **65** 1617
[29] Pendry J B 1994 *J. Mod. Opt.* **41** 209
[30] Ozbay E, Tuttle G, Mccalmont J S, Sigalas M, Biswas R, Soukoulis C M and Ho K M 1995 *Appl. Phys. Lett.* **67** 1969
[31] Mekis A, Chen J C, Kurland I, Fan S, Villeneuve P R and Joannapoulos J D 1996 *Phys. Rev. Lett.* **77** 3787
[32] Ozbay E and Temelkuran B 1996 *Appl. Phys. Lett.* **69** 743
[33] Villeneuve P R, Abrams D S, Fan S and Joannopoulos J D 1996 *Opt. Lett.* **21** 2017
[34] Temelkuran B, Ozbay E, Kavanaugh J P, Tuttle G and Ho K M 1998 *Appl. Phys. Lett.* **72** 2376
[35] Loncar M, Nedeljkovic D, Doll T, Vuckovic J, Scherer A and Pearsall T P 2000 *Appl. Phys. Lett.* **77** 1937
[36] Li Z, Aydin K and Ozbay E 2007 *Appl. Phys. Lett.* **91** 121105
[37] Pendry J B 2000 *Phys. Rev. Lett.* **85** 3966
[38] Grbic A and Eleftheriades G V 2004 *Phys. Rev. Lett.* **92** 117403

[39] Lagarkov A N and Kissel V N 2004 *Phys. Rev. Lett.* **92** 077401
[40] Aydin K, Bulu I and Ozbay E 2007 *Appl. Phys. Lett.*
     90 254102
[41] Kik P G, Maier S A and Atwater H A 2004 *Phys. Rev.* B
     69 045418
[42] Fang N, Lee H, Sun C and Zhang X 2005 *Science* **308** 534
[43] Melville D O S and Blaikie R J 2005 *Opt. Express* **13** 2127
[44] Liu Z, Durant S, Lee H, Pikus Y, Fang N, Xiong Y, Sun C and
     Zhang X 2007 *Nano Lett.* **7** 403
[45] Liu Z, Lee H, Xiong Y, Sun C and Zhang X 2007 *Science*
     315 1686
[46] Lee H, Liu Z, Xiong Y, Sun C and Zhang X 2007 *Opt. Express*
     15 15886
[47] Smolyaninov I I, Hung Y J and Davis C C 2007 *Science*
     315 1699
[48] Pendry J B, Schurig D and Smith D R 2006 *Science* **312** 1780
[49] Schurig D, Mock J J, Justice B J, Cummer S A, Pendry J B,
     Starr A F and Smith D R 2006 *Science* **314** 977
[50] Yen T J, Padilla W J, Fang N, Vier D C, Smith D R, Pendry J B,
     Basov D N and Zhang X 2004 *Science* **303** 1494
[51] Linden S, Enkrich C, Wegener M, Zhou J, Koschny T and
     Soukoulis C M 2004 *Science* **306** 1351
[52] Shalaev V M, Cai W, Chettiar U K, Yuan H, Sarychev A K,
     Drachev V P and Kildishev V 2005 *Opt. Lett.* **30** 3356
[53] Zhang S, Fan W, Panoiu N C, Malloy K J, Osgood R M and
     Brueck S R J 2005 *Phys. Rev. Lett.* **95** 137404
[54] Smith D R, Schultz S, Markos P and Soukoulis C M 2002
     Phys. Rev. B **65** 195104
[55] Smith D R, Vier D C, Koschny T and Soukoulis C M 2005
     Phys. Rev. E **71** 036617
[56] Chen X, Grzegorczyk T M, Wu B I, Pacheco J and Kong J A
     Phys. Rev. E **70** 016608